DOI: 10.1002/ejic.200600580

Thermal Evolution of a MgAl Hydrotalcite-Like Material Intercalated with Hexaniobate

Daniel Carriazo,[a] Cristina Martín,[a] and Vicente Rives*[a]

Keywords: Layered double hydroxides / Polyoxometalates / Nb-Mg-Al mesoporous oxides / Intercalations

A MgAl hydrotalcite-like material intercalated with hexaniobate has been prepared by the anion exchange method from the corresponding nitrate precursor; the sample and the oxides obtained upon its calcination were characterized by element chemical analysis, powder X-ray diffraction, thermal analyses (thermogravimetric and differential), nitrogen adsorption-desorption isotherms at –196 °C, transmission electron microscopy, and FT-IR and UV/Vis spectroscopy. The results show the formation of a microporous hydrotalcite-type solid with a gallery height of 7.2 Å where the $H_3Nb_6O_{19}^{5-}$ anions are oriented with their C_3 axes perpendicular to the layers. This material preserves its layered structure upon calcination up to 400 °C; calcination above this temperature causes decomposition of the hexaniobate and the layered structure collapses, giving rise to amorphous mesoporous solids (Nb-Mg-Al-O) with a large specific surface area (157 $m^2 g^{-1}$). At 800 °C crystallization of $Mg_4Nb_2O_9$ takes place. FT-IR studies on the acid-basic properties carried out by pyridine and 2-propanol adsorption, showed that all solids obtained through hydrotalcite calcination present Lewis-type acid and Brönsted-type basic sites.

Introduction

Layered Double Hydroxides (LDHs), also known as hydrotalcite-like compounds or anionic clays, are lamellar materials generally described by the empirical formula $M^{2+}_{1-x}M^{3+}_x(OH)_2(A^{m-})_{x/m}\cdot nH_2O$, where A^{m-} is the anion balancing the net positive charge of the brucite-like layers[1–3] developed by a partial M^{2+}/M^{3+} substitution. A large number of compounds with this structure have been synthesized in the last decades varying the nature and the molar ratio of the cations in the layers and the nature of the interlayer anions. These compounds have shown their suitability in different fields, acting as anion scavengers in wastewater, biomolecule reservoirs or as polymer additives to improve its properties.[4–6] Nevertheless, there is no doubt that it is in the field of catalysis where they find the widest number of applications, as catalysts, catalyst precursors or supports.[7] These last applications are mainly due to the fact that calcination of the mentioned materials gives rise to systems constituted by different phases (mixed metal oxides) which usually show higher stability, larger surface development and longer life-time than others prepared by conventional methods.

Polyoxometalates (POMs) are anionic compounds with a cluster structure formed by linked oxygen octahedra coordinating transition metals (V, Mo, W, isopolyoxometalates), although in many cases a heteroatom (P, Si) in a tetrahedrally coordinated unit is included in the structure (heteropolyoxometalates).[8] These compounds have also deserved much attention because of the multiple applications they find in many different fields, such as medicine, materials science and catalysis.[9–11] POMs containing niobium have been scarcely studied and, contrary to those containing V, Mo or W, are synthesized under basic pH conditions.[12] The best-known niobium POM is hexaniobate ($Nb_6O_{19}^{8-}$), which has the Lindqvist structure, and is obtained through alkaline fusion of Nb_2O_5. Niobium compounds are extensively used in many heterogeneous catalytic processes where they can act as catalyst supports or as the active phase.[13]

In order to modify the textural properties and to develop acid and electron acceptor centres in the hydrotalcite basic structure and thereby improve its catalytic properties, many authors have reported the intercalation of different oxo- or polyoxometalates between the LDH layers,[14,15] giving rise to very selective catalysts in some oxidation reactions such as dehydrogenation or alkene epoxidation.[16–18] In a previous work Evans et al. reported the intercalation of some hexametalates with the Lindqvist structure [$V_2W_4O_{19}^{4-}$ and $Nb_xW_{6-x}O_{19}^{(x+2)-}$ where x = 2, 3, 4] within the interlayers of hydrotalcite,[19] but a study of the intercalation of hexaniobate is lacking in the literature, and so herein we report the synthesis of a new MgAl LDH intercalated with hexaniobate ($H_3Nb_6O_{19}^{5-}$) prepared by anion exchange, starting from a nitrate LDH (MgAl-NO_3) precursor. Its characterization, as well as of the oxides obtained upon its calcination, by element chemical analyses, Powder X-ray Diffraction (PXRD), Thermogravimetric (TG) and Differential

[a] Departamento de Química Inorgánica, Universidad de Salamanca,
37008 Salamanca, Spain

Table 1. Elemental chemical analyses of the prepared samples and their corresponding formulae.

Sample	Mg[a]	Al[a]	N[a]	Nb[a]	K[a]	C[a]	Formula
MgAl-NO_3	18.5	10.1	5.2	–	–	–	$[Mg_{0.67}Al_{0.33}(OH)_2](NO_3)_{0.33}\cdot 0.44H_2O$
$K_8Nb_6O_{19}$	–	–	–	40.0	22.5	–	$K_8Nb_6O_{19}\cdot 13H_2O$
MgAlNb	12.9	6.7	–	25.9	–	0.1	$[Mg_{0.68}Al_{0.32}(OH)_2](H_3Nb_6O_{19})_{0.06}(CO_3)_{0.01}\cdot 0.70H_2O$

[a] Weight percentage.

Thermal Analyses (DTA), nitrogen adsorption-desorption at –196 °C, Scanning and Transmission Electron Microscopy (SEM and TEM), and Fourier Transform Infrared (FT-IR) and Vis-UV spectroscopy are also reported. Crystalline potassium hexaniobate, which was synthesized for preparation of MgAl-hexaniobate LDH, has also been characterized and used as a reference. The acid-base properties of the solids obtained by calcination of the MgAl-hexaniobate LDH were tested by FT-IR spectroscopy after pyridine or 2-propanol adsorption.

Results and Discussion

Element chemical analysis carried out for potassium hexaniobate as well as for both layered samples lead to the following formulae: $K_8Nb_6O_{19}\cdot 13H_2O$, $[Mg_{0.67}Al_{0.33}(OH)_2](NO_3)_{0.33}\cdot 0.44H_2O$ and $[Mg_{0.68}Al_{0.32}(OH)_2](H_3Nb_6O_{19})_{0.06}(CO_3)_{0.01}\cdot 0.70H_2O$, respectively (values have been rounded to two figures after the decimal point) (Table 1). This last formula has been calculated considering $H_3Nb_6O_{19}^{5-}$ as the interlayer anion since this is the predominant species at the pH conditions (12.5) at which the exchange process was performed.[13] The amount of interlayer water (0.70 molecules per LDH mol) has been determined from the TG curve (see below). The slight increase of the Mg/Al molar ratio from 2 (MgAl-NO_3) to 2.1 (MgAlNb) after the exchange process is probably due to a partial dissolution of the aluminum cations as aluminate as a consequence of its amphoteric character and the extremely high pH used during the exchange process to stabilize the niobium POM, although this small difference could also be ascribed to the experimental error of the technique.

It should be mentioned that different intercalation attempts, such as direct synthesis from metal nitrate salts or exchange using meixnerite (a MgAl LDH containing hydroxyl as the interlayer anion) as a precursor were tested and none of them produced the hexaniobate intercalation, the unique layered phase detected using these synthesis routes being hydrotalcite, MgAl-CO_3. Addition of the LDH-NO_3 as a slurry, as recommended by other authors to facilitate anion exchange,[20] was also unsuccessful, probably due to changes in pH leading to Nb_2O_5 precipitation.

Although the procedure followed to synthesize potassium hexaniobate is described in the literature to produce the single-protonated form, element chemical analyses and the PXRD pattern in Figure 1, from comparison with the JCPDS file 14-0288, confirm that the niobium polyoxometalate formed in this case was octo-potassium hexaniobate ($K_8Nb_6O_{19}\cdot 13H_2O$). To study its thermal stability the PXRD patterns of the products obtained upon its calcination at different temperatures were recorded and are also shown in this Figure. As can be observed, potassium hexaniobate completely decomposes below 300 °C and two different crystallographic forms of potassium niobate, $KNbO_3$, have been identified, one at 300 °C and the other at 600 °C, matching with the 32-0821 and 32-0822 JCPDS files, respectively.

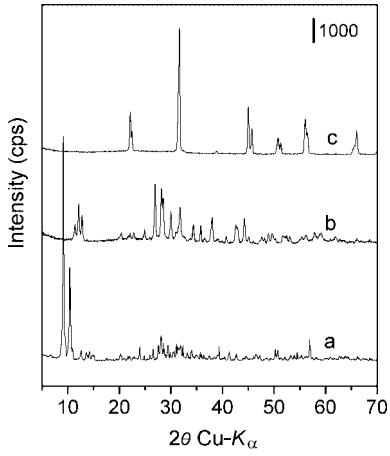

Figure 1. PXRD patterns of $K_8Nb_6O_{19}$ (a) uncalcined, and calcined at (b) 300 °C and (c) 600 °C.

The powder XRD patterns of sample MgAlNb, both original and calcined at increasing temperatures, are shown in Figure 2. The first one is characteristic of materials with the hydrotalcite-like structure in which the intercalation of hexaniobate has led to an increase in the basal spacing from 8.8 Å (corresponding to a phase with intercalated nitrate anions in an upwards configuration) to 12.0 Å, which means a gallery height of 7.2 Å, once the brucite-like layers width (4.8 Å)[21] is subtracted. This value is in agreement with the height of a hexaniobate anion, ($Nb_6O_{19}^{8-}$)[22,23] with its C_3 axis perpendicular to the layers (Figure 3). The basal spacing, usually measured from the d_{003} diffraction peak (assuming a$R\bar{3}m$ layers stacking) was calculated in this sample from the positions of the peaks due to other basal planes, (006) and (009), recorded at 6.0 and 4.0 Å, respectively, because the peak due to (003) planes is partially hidden by a broad peak centred at 11 Å. The pattern is similar to that reported by different authors for other POM-LDHs systems.[20,21,24–31] Regarding the broad reflection between 10–12 Å some authors have claimed that it is produced by a poorly crystallized phase of a M^{2+}/M^{3+}-POM salt in low quantities,[20,26] while other authors have proposed different alternatives.[27–30] The unexpected low intensity of the peak due to diffraction by the (003) planes (weaker than the other two basal reflections recorded) is due to the presence

of species (POMs) with high scattering factors in the interlayers.[29]

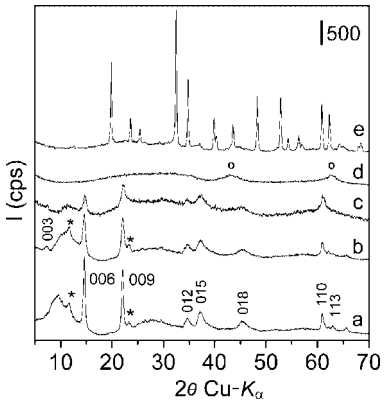

Figure 2. PXRD patterns of samples MgAlNb: (a) uncalcined and calcined at (b) 150 °C, (c) 300 °C, (d) 450 °C and (e) 800 °C. (*) MgAl-CO_3; (o) MgO. Miller indexes are labelled for the layered phase.

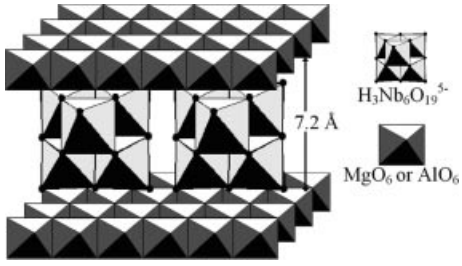

Figure 3. Scheme of MgAl LDH pillared with hexaniobate.

Additionally, and in agreement with the chemical analyses, a small amount of another layered crystalline phase, ascribed to hydrotalcite (MgAl-CO_3), is also present, even though extreme care was taken to avoid CO_2. This phase could have been formed during the exchange process due to the high affinity that these materials have towards carbonate under the strongly basic conditions (pH = 12.5) at which the reaction was carried out, or it could have been incorporated during post-synthesis treatments while the solid was still wet (during washing or drying processes).

The PXRD pattern recorded for the sample calcined at 150 °C (Figure 2, b) is rather similar to that recorded for the uncalcined one, but a decrease in the intensity of the broad peak centred at 11 Å allows the weak (003) reflection to be distinguished at the position expected (12 Å) taking into account the positions of the peaks due to diffraction by planes (006) and (009). The diffractograms are quite similar for samples calcined below 300 °C, although some differences are observed in the PXRD pattern of the sample calcined at 300 °C, Figure 2 (c); the reflections due to the MgAl-CO_3 phase have vanished, and a decrease in the intensities of all the peaks is also observed. The characteristic reflections due to planes (003), (006), (009) and (110) of a hydrotalcite-like material are still observed at 400 °C, which means that the POM ions hosted in the interlayers are thermally more stable than when they are isolated as a potassium salt (decomposition is observed at 300 °C). The PXRD pattern for the sample calcined at 450 °C, Figure 2 (d), is typical of an amorphous material, indicating that the layered structure has collapsed, giving rise to amorphous oxides for which the PXRD diagram shows only weak peaks at 2.1 and 1.5 Å ascribed to the MgO periclase phase (JCPDS file: 4-0829). Similar patterns are observed for samples calcined up to 700 °C, but at 800 °C the PXRD pattern (MgAlNb800, Figure 2, e) shows sharp diffraction maxima characteristic of a crystalline phase ascribed to magnesium niobate, $Mg_4Nb_2O_9$ (JCPDS file: 36-1381). No crystalline phase containing aluminum has been identified at any calcination temperature, suggesting that it must be well dispersed or forming amorphous phases. At these calcination temperatures, the niobium in excess which has not reacted with magnesium (Mg/Nb = 1.8) to form magnesium niobate must be, as well as aluminum, forming an amorphous phase, since no peaks corresponding to crystalline Nb_2O_5 were detected by PXRD.

The FT-IR spectra of potassium hexaniobate and of LDH-niobate (MgAlNb sample) are shown in Figure 4. Apart from the bands due to the LDH matrix, the spectra are very similar, suggesting that the hexaniobate structure is maintained after the exchange. Bands at 3462 cm^{-1} (broad) and at 1640 cm^{-1} for the potassium salt are due to the hydroxyl groups stretching mode and the bending mode of water molecules, respectively. The bands due to Nb=O and Nb–O–Nb stretching vibrations are recorded in the 900–400 cm^{-1} range (844, 697, 528, and 415 cm^{-1}), in agreement with those previously reported elsewhere for this compound.[32] After intercalation into the LDH structure, bands ascribed to Nb–O stretching modes in hexaniobate units (844, 770, and 542 cm^{-1}) are still recorded, together with other bands at 664, 447, and 402 cm^{-1} due to υ(Mg–O) and Mg/Al–OH translational modes of the layers.[33] Another band due to the ν_3 mode of carbonate anions associated to the LDH-carbonate phase identified by XRD is clearly recorded at 1369 cm^{-1}.

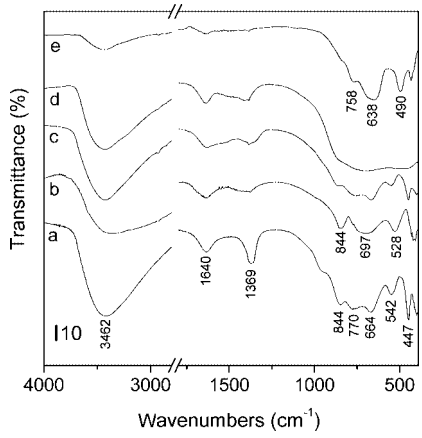

Figure 4. FT-IR spectra of MgAlNb (a) and calcined at (c) 250 °C, (d) 450 °C and (e) 800 °C; (b) FT-IR spectrum of potassium hexaniobate.

The small shift observed for some of the bands ascribed to the hexaniobate unit, when compared with their positions for the potassium salt, is presumably a consequence

of the interaction between the anion and the brucite-like layers.

The FT-IR spectra recorded for calcined MgAlNb samples are also included in Figure 4. Similar spectra to that recorded for the uncalcined sample are observed when the calcination is carried out up to 400 °C, and only an appreciable decrease in the intensity of the bands, especially the one due to carbonate, is observed, in agreement with the PXRD results.

Calcination at 450 °C gives rise to decomposition of hexaniobate and collapse of the layered structure, the spectrum showing a broad band in the 900–400 cm^{-1} range, typical of amorphous oxide species. The spectrum is similar for samples calcined up to 700 °C, but when the solid is calcined at 800 °C, new bands at 758, 638, 490 and 432 cm^{-1} characteristic of the $Mg_4Nb_2O_9$ phase, already identified in this solid by PXRD, develop.

The TG and DTA curves recorded for potassium hexaniobate and the MgAlNb sample are shown in Figure 5. Three thermal effects can be distinguished in the DTA curve of the potassium salt (dashed line in panel A); the first two (at 115 and 290 °C) are endothermic effects and correspond to removal of structural water, the second also coincides with potassium hexaniobate decomposition (observed from the PXRD at 300 °C) to potassium niobate. The exothermic effect recorded at 592 °C can be ascribed to transformation of $KNbO_3$ into another crystalline phase, also observed by PXRD. The TG curve (solid line in panel A) reveals that the structural water, which is the only volatile species in the sample, is lost in different steps. The weight losses represent ca. 16% of the total weight which means 13 water molecules per mol potassium hexaniobate.

Two well-resolved weight losses are recorded in the TG curve for sample MgAlNb (Figure 5B), although the DTA curve shows three endothermic effects; the first one, at 126 °C, can be ascribed to removal of surface adsorbed water. The second effect, at 265 °C is due to removal of interlayer water and the third, recorded at 443 °C, is a consequence of dehydroxylation of the brucite-like layers, matching with the hexaniobate decomposition into amorphous Mg-Al-Nb-O and water, as detected by FT-IR and PXRD between 400 and 450 °C.

Carbonate decomposition to CO_2 around 300 °C, as concluded by PXRD and FT-IR spectroscopy, can be partially included in the peak recorded at 265 °C, although its contribution to the weight loss is almost undetectable due to the low amount of CO_3^{2-} present in the sample. Moreover, the peak at 126 °C could be partially due to the evaporation of some intercalated water, because water adsorbed on the external surface of the crystallites generally is totally evolved at 110 °C. This overlap does not allow ascribing accurately the weight loss to the different processes detected. Consequently, the amount of intercalated water given in the formula of the MgAlNb sample (0.70 molecules per mol of LDH) has been determined in an approximate way from the weight loss recorded between 110 and 270 °C.

The UV/Vis spectra (not shown) recorded for all samples show only an absorption band in the UV range, corresponding to a $Nb^{5+}\leftarrow O^{2-}$ charge-transfer process. A shift from 260 (potassium hexaniobate) to 245 nm (MgAlNb) is observed upon intercalation of hexaniobate in the LDH structure (Table 2). This small hypsochromic shift is probably due to the POM confinement within the layered host. No appreciable change is observed in the spectra of the calcined samples, where only a sharper absorption peak at 253 nm is recorded in the spectrum of the sample calcined at 800 °C (Table 2).

The nitrogen adsorption-desorption isotherm recorded for the MgAlNb sample, Figure 6, previously degassed at 120 °C for 2 h, is in between types I and II of the IUPAC classification,[34] characteristic of microporous solids. The specific surface area determined by the BET method is 24 $m^2 g^{-1}$ (Table 2), 40% of which corresponds to adsorption on micropores (as calculated from the t-plot)[35] and the external surface area corresponds to 14 $m^2 g^{-1}$. Layered double hydroxides intercalated with small anions are not microporous, as the width of the interlayer (ca. 3 Å) is not large enough to host nitrogen molecules. Interlayer micro-

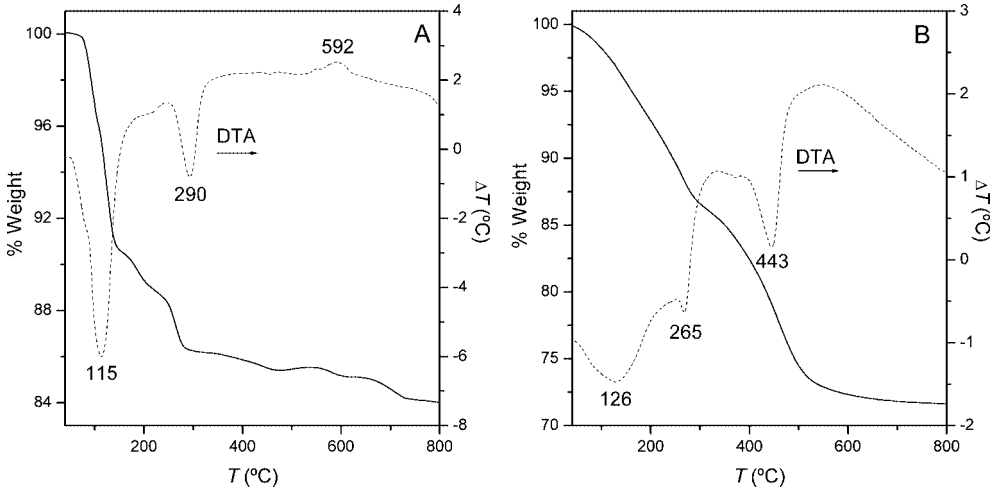

Figure 5. TG (solid lines) and DTA (dotted lines) of (A) potassium hexaniobate and (B) sample MgAlNb, recorded under oxygen.

Table 2. Specific surface areas (S_{BET}: BET method; S_m microporous equivalent surface area, S_{ext} external surface area and V_t total pore volume) and position of the maximum in the UV/Vis spectra for potassium niobate and several layered samples (* determined from the *t*-plot).

Sample	S_{BET}[a]	S_m[a]*	S_{ext}[a]*	V_t[b]	λ[c]
MgAl-NO_3	26	–	27	0.08	–
MgAlNb	24	10	14	0.06	245
MgAlNb500	157	–	160	0.20	239
MgAlNb800	45	6	39	0.12	253
$K_8Nb_6O_{19}$	1	–	–	–	260

[a] $m^2 g^{-1}$. [b] mL g^{-1} (determined at $p/p = 0.95$). [c] nm.

porosity only develops when the interlayers are swelled after intercalation of large anions with a large formal charge, rendering large spaces between them.

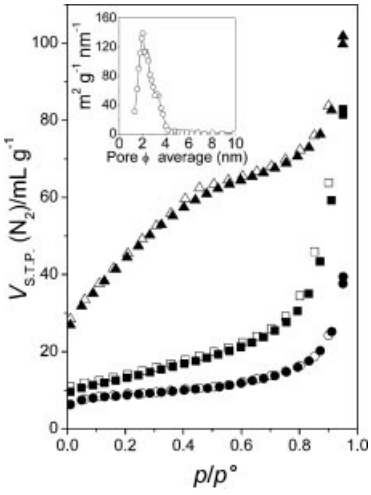

Figure 6. Nitrogen adsorption–desorption isotherms (filled symbols and open symbols, respectively) at –196 °C for the original sample MgAlNb (circles) and calcined at 500 °C (triangles) or 800 °C (squares). The inset shows the pore size distribution for sample MgAlNb500.

The isotherms recorded for the samples calcined between 450 and 600 °C are similar to each other and very different to that recorded for the MgAlNb sample. The isotherm for sample MgAlNb500 (Figure 6) can be classified as type IV, characteristic of mesoporous solids, since it shows a significant increase of the adsorbed amount at an intermediate relative pressure range, produced by a multilayer filling mechanism. The BET surface area for this sample shows an appreciable increase (157 $m^2 g^{-1}$) in comparison to that for the uncalcined one (Table 2). No adsorption on micropores was detected (the zero intercept of the t-plot approached zero) and the corresponding external surface area was calculated as 160 $m^2 g^{-1}$. The pore size distribution plot (Figure 6), shows a very intense and slightly asymmetric curve, which indicates that most of the pores have diameters ranging between 1.8 and 4 nm. A considerable increase in the pore volume (0.20 $cm^3 g^{-1}$) is also observed upon calcination. These textural properties change with calcination above 700 °C. Thus, the MgAlNb800 sample (Figure 6) shows an isotherm similar to that recorded for the pristine layered material. The BET surface area decreases to 45 $m^2 g^{-1}$, probably due to crystallization of magnesium niobate, $Mg_4Nb_2O_9$, (detected by PXRD), although it remains larger than that measured for crystalline potassium hexaniobate and its calcination products (between 1 and 2 $m^2 g^{-1}$), suggesting that other phases corresponding to aluminum-containing amorphous species also exist. For this sample a small fraction of micropores is also found.

Representative scanning and transmission electron micrographs (SEM and TEM) for calcined and uncalcined samples are shown in Figure 7 and Figure 8. At first sight, when potassium hexaniobate crystallizes from solution, enlarged prismatic-shaped crystals are formed. From the SEM micrographs it can be observed that these crystals have a hexagonal section (see parts a and b in Figure 7), and a closer view reveals small, smooth crystalline particles with sizes between 2 and 5 μm (Figure 7, c).

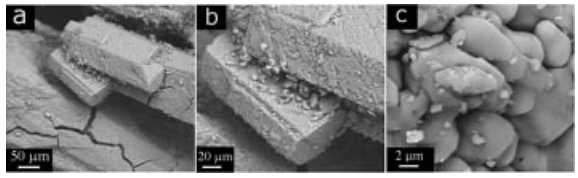

Figure 7. SEM pictures of potassium hexaniobate with different magnification.

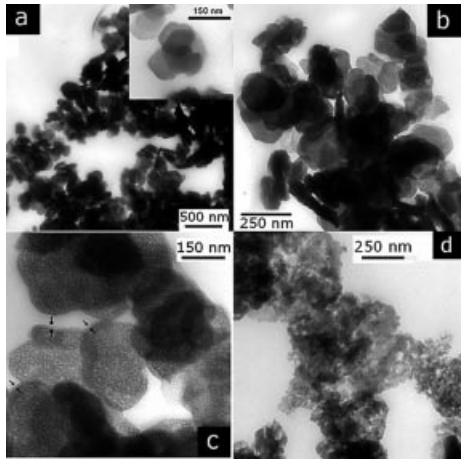

Figure 8. TEM pictures of the original sample MgAlNb (a), inset closer view and calcined at 500 °C (b, c) and 800 °C (d).

The typical hydrotalcite morphology, hexagonal platelet particles, is clearly observed by TEM for the as-synthesized MgAlNb sample (Figure 8, a). The size of the hexagonal crystals is ca. 100 ± 50 nm and their thickness 20 ± 10 nm. Calcination between 450 and 600 °C produces a smoothing of the particle edges (Figure 8, parts b and c), which are now more rounded than those observed for the uncalcined ones. A quite homogeneous pore distribution is simultaneously developed, in agreement with the results obtained by the nitrogen adsorption study. The particles are surrounded by an amorphous wall with a thickness of 10 nm (indicated by arrows in Figure 8, c).

For the sample calcined at 800 °C (Figure 8, d) the morphology completely changes; aggregates of very small irregular-shaped particles (between 20 and 50 nm) are observed, indicating that the magnesium hexaniobate ($Mg_4Nb_2O_9$) phase (detected by PXRD and FT-IR), is well mixed or embedded in an amorphous phase (formed by Al-Nb oxides).

The textural and morphological properties observed for sample MgAlNb calcined between 450 and 600 °C have not been previously reported for LDH-POM calcined systems.[30,36,37] In these last cases, as well as for LDHs intercalated with permanent (nonvolatile) anions, a decrease in the surface areas is usually observed upon calcination. On the other hand, calcination of hydrotalcites intercalated with volatile anions (CO_3^{2-}, NO_3^-, etc.)[36,38] results in the development of porosity and, as a consequence, an enhancement of their surface areas. Different factors influence this process, such as the preparation method, nature of the metal ions in the layers, the sort of anion, etc., and it is ascribed to the evolved gases (NO_2, CO_2, O_2, etc.) produced upon anion decomposition, escaping through the crystal basal faces. However, in previous reports where TEM pictures of calcined hydrotalcites are shown,[36] no particles as well defined as in our case have been observed.

Because of the high basicity of the hexaniobate anion in comparison with other polyoxometalates (heptamolybdate or polyoxotungstates), a delay of the reaction between hexaniobate and the magnesium existing in the layers may be produced, enhancing its thermal stability, so POM decomposition and layer dehydroxylation take place in a narrow temperature range. This may be the reason why an amorphous solid (Mg-Al-Nb-O) with these special textural properties is formed.

Acid-Base Properties

To gain insight into the surface properties of solid MgAlNb500 we have tested its acid-base properties by the adsorption of pyridine and 2-propanol monitored by FT-IR spectroscopy.

Pyridine Adsorption

The FT-IR spectrum of the MgAlNb500 sample after pyridine adsorption at room temperature and outgassing at the same temperature is shown in part A of Figure 9; only bands at 1608, 1586, 1575, 1487 and 1443 cm^{-1} are recorded, ascribed to modes 8a, 8b, 19a and 19b, respectively, of pyridine bonded to surface Lewis acid sites. The splitting observed for the band originated by mode 8a (1608, 1586 cm^{-1}) clearly shows the presence of two different types of surface Lewis acid sites on the surface of this solid. The positions of the bands are similar to those previously recorded upon adsorption of py on alumina, and so the bands here recorded should be ascribed to pyridine adsorbed on tetrahedrally (1608 cm^{-1}) or octahedrally coordinated (1586 cm^{-1}) Al^{3+} cations,[39] although the first one could also be ascribed to py bonded to coordinatively unsaturated (cus) Nb^{5+} ions, since its position coincides with that of the band recorded after adsorption of pyridine on Nb_2O_5.[40] When the outgassing temperature is increased up to 300 °C, Figure 9 (A), the intensity of the bands are markedly reduced, but they are still observed, indicating that the Lewis-type acid centres are strong.

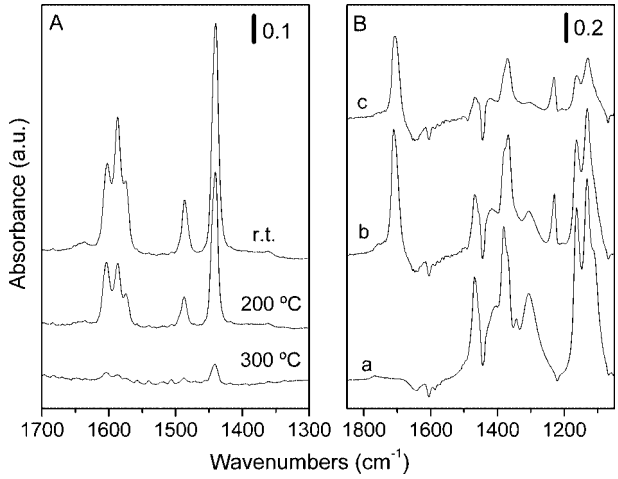

Figure 9. (A) FT-IR spectra of pyridine adsorbed at room temperature on MgAlNb500 and outgassing at the temperatures given (in °C); (B) FT-IR spectra of 2-propanol adsorbed at room temp. on MgAlNb500 (a) and heated at (b) 200 °C and (c) 300 °C.

The FT-IR spectrum of pyridine adsorbed on sample MgAlNb800 (not shown) is similar to that recorded upon adsorption on the sample calcined at 500 °C, where only Lewis acid sites are detected, but they are weaker than for the sample calcined at 500 °C, as they were removed after outgassing merely at 200 °C.

Some authors have reported the existence of Brönsted acid sites in niobium-containing samples when they are exposed to water,[41] but they were not observed in our samples; the FT-IR spectra recorded after adsorption of py on samples previously exposed in situ to water vapour are similar to that recorded for the unwetted samples.

Isopropanol Adsorption

The FT-IR spectrum of 2-propanol (ISP) adsorbed on sample MgAlNb500 at room temperature is displayed in part B of Figure 9. It shows a broad band at ca. 3255 cm^{-1} (not shown) which corresponds to new surface hydroxyl groups developed on the surface of the solid by a dissociative adsorption mechanism. Sharp bands at 2970, 2936, 2878, and 2728 cm^{-1} correspond to stretching modes of the methyl group and the bands in the low wavenumbers region, at 1468, 1382, 1308, 1164, and 1135 cm^{-1} [ascribed to $\delta(CH_3)$, $\nu(CO)$, and $\nu(CC)$], are characteristic of alcoholate species formed via dissociative adsorption of the ISP molecule. When the solid is heated in situ at increasing temperatures, Figure 9 (B), the intensities of the bands originated by the isopropoxide species decrease; new bands develop above 200 °C at 1709 and 1230 cm^{-1}, which correspond to $\nu(C{=}O)$ and $\nu_{as}(C–C–C)$ modes of acetone weakly coordinated through the oxygen atom of the carbonyl group to surface Lewis acid sites. The latter bands disappear upon outgassing at low temperature (100 °C). Adsorption of ISP

on sample MgAlNb calcined at 800 °C (not shown) gives rise to similar spectra, although the bands assigned to acetone are less intense.

ISP decomposition to acetone or propene is considered as a test reaction in the study of the acid-base and redox properties of metal oxide heterogeneous catalysts[42,43] since Brönsted acid sites are needed for propene formation via dehydration, while Lewis-type acid and basic, and redox centres are required for acetone formation via oxidative dehydrogenation, but only acid and basic sites if the acetone is produced via simple dehydrogenation. In our case, formation of acetone (detected by FT-IR) has to be produced through this last process, since temperature programmed reduction (TPR) studies carried out on our samples did not show any hydrogen consumption due to Nb^{5+} reduction. The reaction may proceed through the following steps: (1) ISP is first dissociatively adsorbed on Lewis-type acid sites as an isopropoxide species and the proton is adsorbed on basic centres−surface exposed oxide anions−and (2) the abstraction of a second hydrogen atom from the alcohol takes place. On desorption, acetone and H_2 are the reaction products.

In summary, Lewis-type acid and Brönsted-type basic centres are present in the calcined samples.

Conclusions

All the results reported here support the successful intercalation for the first time of hexaniobate between the MgAl brucite-like layers, rendering a new microporous layered material which retains its structure during calcination in air up to 400 °C, i.e., an enhancement in POM thermal stability is achieved upon its intercalation. Calcination at 450 °C produces dehydroxylation of the layered structure and POM decomposition, giving rise to amorphous mesoporous solids, with a large specific surface area (157 $m^2 g^{-1}$); further calcination at 800 °C leads to magnesium niobate crystallization which is embedded in an amorphous Nb-Al-containing phase. All calcined solids show surface Lewis-type acid and Brönsted-type basic sites, which are responsible for acetone formation by simple dehydrogenation of 2-propanol.

In addition to succeeding in preparing a novel, thermally stable MgAl-hexaniobate LDH, an amorphous mesoporous solid, Mg-Al-Nb-O, which seems suitable to be used as a catalyst support or adsorbent, was formed through its calcination between 450–600 °C.

Experimental Section

All reagents were purchased from Aldrich and used without any further purification.

Potassium hexaniobate ($K_8Nb_6O_{19}·13H_2O$) was synthesized following a preparation method similar to that described elsewhere;[44] Nb_2O_5 (13.3 g, 50 mmol) was slowly added to a KOH (26 g, 394 mmol) melt in a nickel crucible; once the addition was completed the mixture was further heated for 30 min and then it was poured into decarbonated water (100 mL). After filtering the solution the volume was reduced to 50 mL and the solution was cooled overnight at 0 °C. The crystals that formed were filtered off and washed with a 1:1 (v/v) ethanol/water mixture and dried under vacuum in a desiccator.

The MgAl-NO_3 hydrotalcite−$Mg_2Al(OH)_6(NO_3)·1.33H_2O$−was prepared by coprecipitation from the corresponding metal nitrate salts, following a method previously described:[45] a solution formed by dissolving $Mg(NO_3)_2·6H_2O$ (12.8 g, 50 mmol) and $Al(NO_3)_3·9H_2O$ (9.4 g, 25 mmol) in water (150 mL) was added dropwise under nitrogen to CO_2-free water (150 mL). The pH was maintained close to 10 by simultaneous addition of a 2-M NaOH solution, and the mixture was stirred for 24 h at room temperature and then it was treated for five days at 70 °C under hydrothermal conditions in a Teflon-lined steel autoclave at autogenous pressure. The suspension was finally washed with decarbonated water, centrifuged and dried under vacuum.

The MgAl-hexaniobate LDH was prepared by anion exchange, by adding dry $Mg_2Al(OH)_6(NO_3)·1.33H_2O$ (1.0 g, 3.8 mmol) to a solution of $K_8Nb_6O_{19}·13H_2O$ (1.5 g, 1.1 mmol) in CO_2-free water (70 mL). The pH finally achieved was 12.5. The mixture was kept under nitrogen and refluxed at 90 °C for 6 h; the resulting solid was centrifuged and washed with boiling water and finally dried under vacuum in a desiccator. The sample obtained in this way is designated as MgAlNb, and the samples obtained upon calcination are labelled as MgAlNbT (where *T* is the calcination temperature in °C).

Instrumentation: Element chemical analyses were carried out in Servicio General de Análisis Químico Aplicado (University of Salamanca, Spain); Mg, Al and Nb were determined by atomic absorption in a Mark-2 EEL 240 apparatus, while carbon and nitrogen contents were determined with a CHNS 932 Leco analyzer.

The powder X-ray diffraction (PXRD) patterns were obtained with a Siemens D-500 diffractometer, using Cu-$K_{\alpha 1}$ radiation (λ = 1.54050 Å).

Differential thermal analysis (DTA) and thermogravimetric (TG) analysis curves were recorded in DTA-7 and TG-7 instruments, respectively, from Perkin–Elmer. The analyses were carried out in flowing (30 mL min^{-1}) oxygen from L'Air Liquide (Spain) at a heating rate of 10 °C min^{-1}.

The nitrogen adsorption-desorption isotherms for specific surface area measurements were recorded at –196 °C in a Gemini instrument from Micromeritics. The samples were previously outgassed at 120 °C for 2 h. The pore size distribution plotted for MgAlNb500 was obtained from the Cranston and Inkley method.[46]

The UV/Vis spectra were recorded in the 200–1100 nm range with a Perkin–Elmer Lambda 35 apparatus equipped with a Labsphere RSA-PE-20 accessory by the diffuse reflectance technique; MgO was used as a reference.

Fourier Transform infrared spectra (FT-IR) were collected with a Perkin–Elmer FT-1730 instrument using the KBr pellet technique.

The FT-IR technique was also used to assess the surface acidity/basicity properties using pyridine or 2-propanol as probe molecules. These spectra were recorded with a Perkin–Elmer 16 PC spectrometer using self-supported discs; the sample was degassed in situ in a special cell[47] with CaF_2 windows at 400 °C for 2 h at 10^{-4} N m^{-2}, prior to the adsorption experiments. After degassing, the probe molecule vapour was adsorbed at room temperature and, in the case of pyridine (py), the spectra were recorded after outgassing at increase temperatures (from room temp. to 400 °C), while

2-propanol (ISP) was adsorbed at room temp. and, without removing the gas phase, the solid was heated at increasing temperatures (100–400 °C).

Scanning electron micrographs (SEM) were obtained with a model 940 Digital Scanning-Microscope from Zeiss.

Transmission electron micrographs (TEM) were obtained with a Zeiss-902 apparatus equipped with a digital camera, the samples were prepared on a copper grid after evaporating a drop of sample dispersed in water.

Acknowledgments

The authors acknowledge financial support from MEC (grant MAT2003-06605-C02-01) and ERDF; DC also thanks a grant from Universidad de Salamanca.

[1] V. Rives (Ed.), *Layered Double Hydroxides: Present and Future*, Nova Science Publishers, Inc., New York, **2001**.
[2] E. Wypych, K. G. Satyanarayana (Eds.), *Clay Surfaces: Fundamental and Applications*, Elsevier, Amsterdam, **2004**.
[3] D. G. Evans, R. C. T. Slade, *Struct. Bond.* **2006**, *119*, 1–87.
[4] N. K. Lazaridis, T. A. Pandi, K. A. Matis, *Ind. Eng. Chem. Res.* **2004**, *43*, 2209–2215.
[5] J. H. Choy, S. Y. Kwak, Y. J. Jeong, J. S. Park, *Angew. Chem. Int. Ed.* **2000**, *39*, 4042–4045.
[6] L. Li, R. Z. Ma, Y. Ebina, N. Iyi, T. Sasaki, *Chem. Mater.* **2005**, *17*, 4386–4391.
[7] S. Albertazzi, F. Basile, A. Vaccari in *Clay Surfaces: Fundamental and Applications* (Eds.: E. Wypych, K. G. Satyanarayana), Elsevier, Amsterdam, **2004**, p. 497–546.
[8] M. T. Pope, *Heteropoly and Isopoly Oxometalates*; Springer-Verlag, New York **1983**.
[9] I. V. Kozhevnikov, *Chem. Rev.* **1998**, *98*, 171–198.
[10] N. Mizuno, M. Misono, *Chem. Rev.* **1998**, *98*, 199–217.
[11] J. T. Rhule, C. L. Hill, D. A. Judd, R. F. Schinazi, *Chem. Rev.* **1998**, *98*, 327–357.
[12] M. Nyman, F. Bonhomme, T. M. Alam, M. A. Rodriguez, B. R. Cherry, J. L. Krumhansl, T. M. Nenoff, A. M. Sattler, *Science* **2002**, *297*, 996–998.
[13] I. Nowak, M. Ziolek, *Chem. Rev.* **1999**, *9*, 3603–3624.
[14] T. Kwon, G. A. Tsigdinos, T. J. Pinnavaia, *J. Am. Chem. Soc.* **1988**, *110*, 3653–3654.
[15] V. Rives, M. A. Ulibarri, *Coord. Chem. Rev.* **1999**, *181*, 61–120.
[16] B. F. Sels, D. E. de Vos, P. A. Jacobs, *Angew. Chem. Int. Ed.* **2005**, *44*, 310–313.
[17] T. Tatsumi, K. Yamamoto, H. Tajima, H. Tominaga, *Chem. Lett.* **1992**, *5*, 815–818.
[18] E. Gardner, T. J. Pinnavia, *Appl. Catal. A* **1998**, *167*, 65–74.
[19] J. Evans, M. Pillinger, J. J. Zhang, *J. Chem. Soc., Dalton Trans.* **1996**, 2963–2974.
[20] S. K. Yun, T. J. Pinnavaia, *Inorg. Chem.* **1996**, *35*, 6853–6860.
[21] M. A. Drezdzon, *Inorg. Chem.* **1988**, *27*, 4628–4632.
[22] I. Lindqvist, *Arkiv Kemi* **1953**, *5*, 247–250.
[23] R. Rhomer, J. E. Guerchais, *Bull. Soc. Chim. Fr.* **1961**, 324–334.
[24] M. R. Weir, J. Moore, R. A. Kydd, *Chem. Mater.* **1997**, *9*, 1686–1690.
[25] M. R. Weir, R. A. Kydd, *Inorg. Chem.* **1998**, *37*, 5619–5624.
[26] E. Narita, P. D. Kaviratna, T. J. Pinnavaia, *J. Chem. Soc., Chem. Commun.* **1993**, 60–62.
[27] J. D. Wang, Y. Tian, R. C. Wang, A. Clearfield, *Chem. Mater.* **1992**, *4*, 1276–1282.
[28] R. S. Weber, P. Gallezot, F. Lefebvre, S. L. Suib, *Microporous Mater.* **1993**, *1*, 223–227.
[29] T. Hibino, A. Tsunashima, *Chem. Mater.* **1997**, *9*, 2082–2089.
[30] M. del Arco, D. Carriazo, S. Gutiérrez, C. Martín, V. Rives, *Inorg. Chem.* **2004**, *43*, 375–384.
[31] F. L. Sousa, M. Pillinger, R. A. S. Ferreira, C. M. Granadeiro, A. M. V. Cavaleiro, J. Rocha, L. D. Carlos, T. Trindade, H. I. S. Nogueira, *Eur. J. Inorg. Chem.* **2006**, *4*, 726–734.
[32] F. J. Farrell, V. A. Maroni, T. G. Spiro, *Inorg. Chem.* **1969**, *8*, 2638–2642.
[33] J. T. Kloprogge, L. Hickey, R. L. Frost, *J. Raman Spect.* **2004**, *35*, 967–974.
[34] K. S. W. Sing, D. H. Everett, R. A. W. Haul, L. Moscou, R. Pierotti, J. Rouquerol, T. Sieminiewska, *Pure Appl. Chem.* **1985**, *57*, 603–619.
[35] B. C. Lippens, J. H. de Boer, *J. Catal.* **1965**, *4*, 319–323.
[36] V. Rives in *Layered Double Hydroxides: Present and Future* (Ed.: V. Rives), Nova Sci. Pub. Inc., New York, **2001**, p. 229–250, and references therein.
[37] D. Carriazo, C. Domingo, C. Martín, V. Rives, *Inorg. Chem.* **2006**, *45*, 1243–1251.
[38] W. T. Reichle, S. Y. Kang, D. S. Everhardt, *J. Catal.* **1986**, *101*, 352–369.
[39] C. Morterra, S. Coluccia, E. Garrone, G. Ghiotti, *J. Chem. Soc., Faraday Trans. 1* **1979**, *75*, 289–304.
[40] C. Martín, G. Solana, P. Malet, V. Rives, *Catal. Today* **2003**, *78*, 365–376.
[41] C. L. T. da Silva, V. L. L. Camorim, J. L. Zotin, M. L. R. D. Pereira, A. D. Faro, *Catal. Today* **2000**, *57*, 209–217.
[42] B. Grzybowska-Swierkosz, *Mater. Chem. Phys.* **1987**, *17*, 121–144.
[43] M. Ai, *J. Catal.* **1977**, *49*, 305–312.
[44] M. Filowitz, R. K. C. Ho, W. G. Klemperer, W. Shum, *Inorg. Chem.* **1979**, *18*, 93–103.
[45] M. del Arco, S. Gutiérrez, C. Martín, V. Rives, J. Rocha, *J. Solid State Chem.* **2000**, *151*, 272–280.
[46] R. W. Cranston, F. A. Inkley, *Adv. Catal.* **1957**, *9*, 143–154.
[47] V. Rives, C. Martín, A. Montero, Spanish Patent, 200100688, **2001**.

Received: June 20, 2006
Published Online: September 22, 2006

